KeAi
CHINESE ROOTS
GLOBAL IMPACT

Available online at www.sciencedirect.com

ScienceDirect

Advances in Climate Change Research 14 (2023) 691−706

www.keaipublishing.com/en/journals/accr/

Assessing CMIP6 simulations of Arctic sea ice drift: Role of near-surface wind and surface ocean current in model performance

Xue WANG[a,b], Ran LU[a,b], Shao-Yin WANG[a,b], Run-Tong CHEN[a,b], Zhuo-Qi CHEN[a,b], Feng-Ming HUI[a,b], Hua-Bing HUANG[a,b], Xiao CHENG[a,b,*]

[a] *School of Geospatial Engineering and Science, Sun Yat-sen University, and Southern Marine Science and Engineering Guangdong Laboratory (Zhuhai), Zhuhai 519082, China*

[b] *Key Laboratory of Comprehensive Observation of Polar Environment (Sun Yat-sen University), Ministry of Education, Zhuhai 519082, China*

Received 15 April 2023; revised 16 July 2023; accepted 18 September 2023
Available online 22 September 2023

Abstract

Sea ice drift is a critical parameter for understanding the rapid changes in Arctic sea ice. Since the release of the Coupled Model Intercomparison Project Phase 6 (CMIP6), there has been a lack of quantitative analysis regarding CMIP6's simulation of Arctic sea ice drift. This study aims to assess the simulated Arctic sea ice drift from 1979 to 2014 by fifteen CMIP6 models against recent satellite retrievals, utilizing various quantitative indices. Additionally, the influence of near-surface wind and surface ocean current on model performance is further analyzed. The CMIP6 models capture several aspects of the observed Arctic sea ice drift climatology and variability. The seasonal patterns of sea ice drift speed in all models exhibit similarities with the observed data, and the models agree with the evaluation datasets, indicating that the seasonal evolution of sea ice drift corresponds to near-surface wind patterns. However, notable discrepancies are identified. All models overestimate sea ice drift speed, exceeding the observational data by 36%−97%. Fourteen out of fifteen models display larger seasonal variability (ranging from 0.74 to 1.28 km d^{-1}) compared to the observed data (0.54 km d^{-1}). Seven out of fifteen models exhibit a significant increasing trend in annual sea ice drift speed, similar to the observed trend of 0.58 km d^{-1} per decade, but with weaker trends (ranging from 0.11 to 0.33 km d^{-1} per decade). The remaining eight models reveal no statistically significant trend. The potential causes of such biases were further explored in this study. It suggests that the overestimation of sea ice drift speed in the models might be primarily attributed to the overestimation of near-surface wind speeds and their influence on sea ice drift speed. The models' overestimation of seasonal variability in near-surface wind speeds may account for the overestimation of seasonal variability in sea ice drift. The models' inability to represent the trend in sea ice drift speed may result from their failure to simulate an increasing trend in surface ocean current speed.

Keywords: Arctic sea ice drift; CMIP6; Model evaluation; Near-surface wind; Surface ocean current

1. Introduction

Arctic sea ice, recognized as an essential component of the global climate system, significantly influences oceanic and atmospheric circulation, thermohaline circulation, and the global heat balance through thermodynamic and dynamic processes (de Vernal et al., 2020; Sévellec et al., 2017; Vihma, 2014). Driven by wind and ocean currents, sea ice drift serves

* Corresponding author. School of Geospatial Engineering and Science, Sun Yat-sen University, and Southern Marine Science and Engineering Guangdong Laboratory (Zhuhai), Zhuhai 519082, China.
E-mail address: chengxiao9@mail.sysu.edu.cn (CHENG X.).
Peer review under responsibility of National Climate Center (China Meteorological Administration).

https://doi.org/10.1016/j.accre.2023.09.005

as a crucial dynamic parameter of sea ice (Dewey et al., 2018; Olason and Notz, 2014; Tremblay and Mysak, 1997), altering its spatial distribution and impacting the mass balance of sea ice as well as the exchange of momentum, heat, and mass among ocean, sea ice, and atmosphere (Kwok et al., 2013). The Beaufort Gyre and the Transpolar Drift represent two prominent large-scale patterns of Arctic sea ice drift (Colony and Thorndike, 1984; Yu et al., 2022). Since the mid-20th century, an increase in the drift speed of Arctic sea ice has been observed (Hakkinen et al., 2008; Spreen et al., 2011). The export volume of ice through the Fram Strait, driven by the Transpolar Drift Stream, has been escalating at a rate of 6% per decade (Smedsrud et al., 2017). Concurrently, the summer sea ice extent in the Beaufort Sea has been diminishing at a rate of 5.9% per decade, with the rate of decline for multi-year ice proving even more pronounced, amounting to 16% per decade (Derksen et al., 2012).

Due to the important role played by Arctic sea ice in rapid climate change, assessing Arctic sea ice drift simulations in coupled global climate models is crucial. This allows for improvements in the representation of physical processes in the Arctic Ocean and reductions in the uncertainties associated with projections of future climate change. Rampal et al. (2011) studied Arctic sea ice models within the phase 3 of the Coupled Model Intercomparison Project (CMIP3), revealing that most models displayed a weak coupling between sea ice state (thickness and ice concentration) and ice velocity, which led to significant biases in the simulation of Arctic sea ice export from 1950 to 2050. Subsequent coupled climate models have shown significant improvements in simulating sea ice drift. Docquier et al. (2017) evaluated the global ocean−sea ice coupled model Nucleus for European Modelling of the Ocean coupled to the Louvain-laNeuve Sea Ice Model (NEMO-LIM3.6) using satellite, buoy, submarine observations and reanalysis data from 1979 to 2013. They found that the model exhibited a reasonable reproduction of the seasonal cycle of sea ice drift speed. Furthermore, the model was observed to effectively capture the relationships between the seasonal cycles of sea ice drift speed, concentration, and thickness, in agreement with observations. Tandon et al. (2018) assessed the long-term relationship between Arctic sea ice drift and ice loss in CMIP5 models. Their findings indicated that the use of consistent temporal sampling led to an increased level of agreement between the sea ice drift speeds estimated from model simulations and observational data, relative to previous studies. Most CMIP5 models qualitatively reproduced the long-term growth trend in the annual average drift speed of Arctic sea ice, with better agreement for winter trends and poorer agreement for summer trends. Some models reproduce the observed behavior where the seasonal cycle of sea ice drift is not driven by the seasonal cycle of near-surface wind, while the other models show sea ice drift speeds that are more in phase with near-surface winds. Yu et al. (2020) evaluated the sea ice drift speed simulation results from the coupled model HIRHAM−NAOSIM 2.0, which consists of the regional atmospheric model HIRHAM5 (a subset of the HIRLAM (High Resolution Limited Area Model) and ECHAM (European Centre Hamburg general circulation model) models) and the regional ocean−sea ice model NAOSIM (North Atlantic/Arctic Ocean Sea Ice Model). Their findings revealed a successful reproduction of summer and autumn drift speeds compared to satellite observations, while a significant overestimation of winter and spring drift speeds was observed. In summer and autumn seasons, the model's results exhibited a realistic negative correlation between drift speed and sea ice thickness, as well as concentration. Nonetheless, this correlation was weaker than the observed results. The model was able to replicate the positive correlation between drift speed and near-surface wind speed, but overestimated the correlation during low-wind conditions when compared to observation/reanalysis data. The sensitivity experiment they conducted showed that accounting for sea ice form drag effects resulted in increased air-to-ice momentum flux and sea ice drift over most of the Arctic, but did not lead to an improvement in the agreement between the modeled drift speed/wind speed ratio and observation/reanalysis data. Yu et al. (2022) assessed Arctic sea ice drift simulation from 1979 to 2014 using nine models from China that participated in CMIP6. While most of the models were able to reasonably represent the spatial patterns of the Beaufort Gyre and Transpolar Drift Stream in their long-term mean sea ice drift, there were variations in the detailed location, extent, and strength. Additionally, around two-thirds of the models were found to simulate the correlation between sea ice drift speed and near-surface wind speed that is consistent with observation/reanalysis data, but about the same proportion of the models failed to replicate the inconsistency between the observed sea ice drift speed and surface ocean current pattern. Notably, none of the nine models captured the widespread acceleration in sea ice drift speed across the Arctic that was observed.

Following the release of CMIP6, there has been a lack of quantitative analysis on the Arctic sea ice drift stimulation from CMIP6, which hinders our understanding of the modeling capability in simulating sea ice drift. Therefore, this study aims to expand the evaluation of Arctic sea ice drift simulations in CMIP6 models by assessing and comparing the historical runs of fifteen models (i.e. 1979−2014) using quantitative indices, including sea ice drift error, sea ice area flux through the Fram Strait, and the maximum rotation in the Beaufort Gyre. Additionally, this study analyzed the influence of near-surface wind and surface ocean current on the model performance.

2. Data and methods

2.1. Model data

Fifteen coupled models participating in the CMIP6 were evaluated, which include CESM2, CESM2-WACCM, CESM2-WACCM-FV2, CMCC-CM2-SR5, CMCC-ESM2, E3SM-1-0, EC-Earth3, EC-Earth3-AerChem, EC-Earth3-CC, EC-Earth3-Veg, EC-Earth3P, HadGEM3-GC31-MM, MRI-ESM2-0, NorESM2-MM, and SAM0-UNI-CON. These

fifteen models were selected due to their comprehensive results for sea ice drift evaluation, providing data on monthly sea ice drift speed, sea ice concentration, near-surface wind speed, and surface ocean current speed across the entire Arctic region. Detailed information about these coupled models can be found in Table A1. Historical simulations from 1979 to 2014 were used for evaluation, in alignment with the available time coverage of satellite-derived sea ice drift data employed for evaluation. The projections of all simulation results were unified to the NSIDC EASE-Grid North, consistent with the projection of the satellite-derived sea ice drift product. The spatial resolution was standardized to 100 km, as most simulations are at a resolution of around 100 km.

2.2. Datasets for evaluation

The evaluation was conducted using the daily Polar Pathfinder sea ice motion vectors with a spatial resolution of 25 km (hereafter referred to as NSIDC-Pathfinder), monthly Bootstrap sea ice concentration with a spatial resolution of 25 km (hereafter referred to as NSIDC-SIC) from the National Snow and Ice Data Center (NSIDC), monthly mean 10-m wind speed and direction data with a spatial resolution of 0.25° from the fifth-generation atmospheric reanalysis dataset (ERA5) released by the European Centre for Medium-Range Weather Forecasts (ECMWF), and monthly mean current speed and direction data with a spatial resolution of 0.25° from Ocean ReAnalysis System 5 (ORAS5). All evaluation data were reprojected to the NSIDC EASE-Grid north with a spatial resolution of 100 km, and the temporal resolution was unified to month, consistent with simulation results.

2.3. Methods

2.3.1. Error estimation

The error of different models was evaluated by calculating the mean error (ME) of speed and mean absolute error (MAE) of speed and angle for the sea ice drift vector, which were then compared to the NSIDC-Pathfinder data. ME and MAE can be given by

$$V_{\mathrm{ME}} = \frac{\sum (V_{\mathrm{m}} - V_{\mathrm{o}})}{N} \tag{1}$$

$$V_{\mathrm{MAE}} = \frac{\sum |V_{\mathrm{m}} - V_{\mathrm{o}}|}{N} \tag{2}$$

$$\theta_{\mathrm{MAE}} = \frac{\sum \Delta\theta}{N} \tag{3}$$

$$\Delta\theta = \begin{cases} |\theta_{\mathrm{m}} - \theta_{\mathrm{o}}| , & |\theta_{\mathrm{m}} - \theta_{\mathrm{o}}| < 180^{\circ} \\ 360^{\circ} - |\theta_{\mathrm{m}} - \theta_{\mathrm{o}}| , & |\theta_{\mathrm{m}} - \theta_{\mathrm{o}}| > 180^{\circ} \end{cases} \tag{4}$$

where V_{ME} represents the ME of speed between different models and NSIDC-Pathfinder data. V_{MAE} and θ_{MAE} denote the MAE of speed and angle, respectively. V_{m} and V_{o} correspond to the sea ice drift speed of the model data and NSIDC-Pathfinder data, respectively. $\Delta\theta$ represents the angle difference between the model data and NSIDC-Pathfinder data. θ_{m} and θ_{o} represent the angle of sea ice drift vectors for model data and NSIDC-Pathfinder data, respectively. N represents the number of drift vectors.

2.3.2. Sea ice area flux through the Fram Strait

To evaluate the simulation performance of various models in representing sea ice movement influenced by the Transpolar Drift Stream, the sea ice area flux through the Fram Strait was calculated and compared between satellite products and different model simulation results. The fluxgate is located at 81°N and spans approximately 400 km (Kwok and Rothrock, 1999), connecting the northeast of Greenland and the northwest of the Svalbard Islands (Fig. 1). The sea ice area flux can be given by

$$F = W \sum_{i=1}^{M-1} s_i c_i \ (i = 1, 2, \cdots, M-1) \tag{5}$$

where F denotes the sea ice area flux, W represents the width of the grid, M refers to the total number of grids in the fluxgate, s_i is the speed of ice motion normal to the exchange gate, and c_i corresponds to the sea ice concentration at the grid point.

2.3.3. The maximum rotation in the Beaufort Gyre

A quantification index termed ‘maximum rotation’ was designed to assess the performance of various models in simulating the Beaufort Gyre-induced sea ice movement. It should be noted that only angles of the sea ice drift were considered for rotation calculation; thus, the rotation was

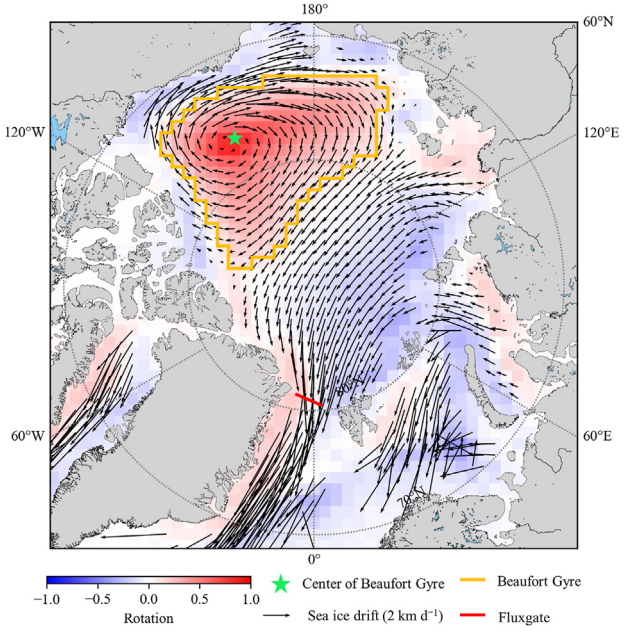

Fig. 1. Fluxgate location used to estimate the Fram Strait sea ice area flux and the Beaufort Gyre extent.

calculated based on the unit sea ice drift vector, which can be given by

$$r = \frac{\partial u_i}{\partial y} - \frac{\partial v_i}{\partial x} \quad (6)$$

where r is the rotation of the grid point, while u and v are the scalar values of the unit sea ice drift vector i in the x and y directions, respectively. The grid point with the maximum rotation value within the extent of the Beaufort Gyre is considered as the center of the Beaufort Gyre, and this maximum rotation value represents the extent of angular differences in sea ice drift at the center of the Beaufort Gyre. The maximum rotation value, which ranges between −1 and 1, should be positive due to the clockwise rotation of the Beaufort Gyre-induced sea ice movement. A value closer to 1 indicates a spatial pattern of sea ice drift near the rotation center that more closely approximates a perfect circular shape. The long-term (1979−2014) mean sea ice drift derived from NSIDC-Pathfinder was utilized to determine the extent of the Beaufort Gyre. Initially, the rotation of each grid was obtained from the mean sea ice drift results. Subsequently, the region exhibiting rotation values exceeding 0.1 and featuring contiguous grid points was identified as the extent of the Beaufort Gyre (Fig. 1).

3. Evaluation of the simulated sea ice drift

3.1. Mean sea ice drift

3.1.1. Monthly and grid-scale view

In Table 1, sea ice drift errors in speed and angle are presented for fifteen models, derived from monthly data across all grid cells. The monthly sea ice drift speed MEs of these models range from 0.48 to 3.12 km d^{-1}, indicating a consistent overestimation of sea ice drift speed across all models. The speed MAEs vary from 2.45 to 4.01 km d^{-1}, while angle MAEs range from 67.09° to 74.86°. Among the models, SAM0-UNICON and HadGEM3-GC31-MM demonstrate significantly superior performance in terms of speed ME and MAE, with noticeably lower values compared to the other models. HadGEM3-GC31-MM also outperforms the other models in angle MAE, whereas the remaining models exhibit similar performance in simulating sea ice drift angle. In terms of speed ME and MAE, SAM0-UNICON achieves the lowest values, 0.48 and 2.45 km d^{-1}, respectively. However, its angle MAE, at 73.63°, is the second highest among the models. HadGEM3-GC31-MM attains comparable speed ME and MAE values (i.e., 0.50 and 2.49 km d^{-1}, respectively) to SAM0-UNICON and exhibits the best accuracy in sea ice drift angle simulation (i.e., 67.09°). Consequently, the HadGEM3-GC31-MM model demonstrates the best overall performance in simulating sea ice drift in terms of speed and angle.

Table 1
Sea ice drift errors for fifteen models.

Model	V_{ME} (km d^{-1})	V_{MAE} (km d^{-1})	θ_{MAE} (°)
CESM2	1.35	2.84	72.27
CESM2-WACCM	1.21	2.75	70.63
CESM2-WACCM-FV2	1.10	2.73	72.40
CMCC-CM2-SR5	2.78	3.81	71.08
CMCC-ESM2	3.12	4.01	70.41
E3SM-1-0	1.43	2.88	74.86
EC-Earth3	1.67	3.09	71.95
EC-Earth3-AerChem	1.65	3.08	71.91
EC-Earth3-CC	2.31	3.49	71.96
EC-Earth3P	1.57	3.02	73.63
EC-Earth3-Veg	1.91	3.31	70.72
HadGEM3-GC31-MM	0.50	2.49	67.09
MRI-ESM2-0	1.96	3.30	72.63
NorESM2-MM	0.82	2.65	71.57
SAM0-UNICON	0.48	2.45	73.33

The boxplots in Fig. 2 present sea ice drift speeds from monthly NSIDC-Pathfinder data and fifteen CMIP6 models, based on all grid points. NSDIC-Pathfinder data presents an average value of 3.50 km d^{-1}, which is significantly lower than those simulated by fifteen CMIP5 models (from 4.77 to 7.10 km d^{-1}). This finding suggests that the sea ice drift speeds in all models are overestimated. In terms of mean, median, lower quartile, and upper quartile values, it is found that the HadGEM3-GC3-MM model exhibits a higher degree of accuracy in relation to NSIDC's values compared to the other models.

3.1.2. Annual and region-scale view

Table 2 presents the 1979−2014 mean of pan-Arctic averaged sea ice drift speed, the maximum rotation in the Beaufort Gyre, and sea ice area flux through the Fram Strait for NSIDC and fifteen models. The annual sea ice area flux through the Fram Strait is derived from the sum of its monthly fluxes. The annual maximum rotation is calculated using annual sea ice drift data, obtained by averaging monthly drift values for each grid cell. Regarding the 1979−2014 mean of pan-Arctic averaged sea ice drift speed, all models consistently overestimate this value. The NSIDC-Pathfinder's 1979−2014 mean drift speed is 3.51 km d^{-1}, while the models' speeds range from 4.76 to 6.93 km d^{-1} (exceeding the observational data by 36%−97%). HadGEM3-GC31-MM's simulation result most closely aligns with the NSIDC-Pathfinder value. For the 1979−2014 mean of sea ice area flux through the Fram Strait, the NSIDC satellite-derived datasets yield a value of 0.58 × 10^6 km^2, while the models' values range from (0.27−0.80) × 10^6 km^2, exhibiting a percentage absolute relative bias (ARB) range of 5%−53%. Six models (i.e. CESM2, CESM2-WACCM, CESM2-WACCM-FV2, E3SM-1-0, EC-Earth3, EC-Earth3-AerChem) show a percentage ARB of no more than 20%. Three models (i.e., CESM2-WACCM-FV2, CMCC-CM2-SR5, CMCC-ESM2) underestimate the 1979−2014 mean of sea ice area flux through the Fram Strait, while the other twelve overestimate it. EC-Earth3's simulation result is the closest to the satellite-derived value. In terms of the 1979−2014 mean maximum rotation in the Beaufort Gyre, NSIDC-Pathfinder obtains a value of 0.83, whereas all models present overestimated simulations ranging from 0.87 to 0.95 (exceeding the

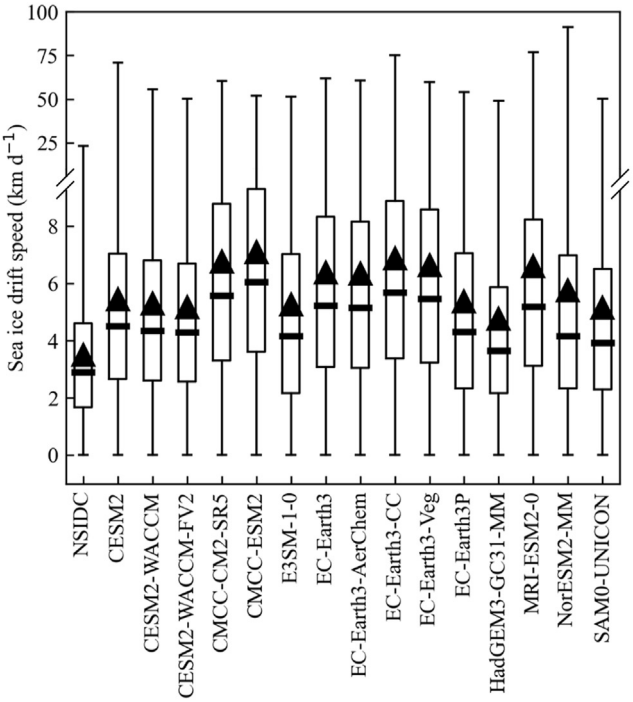

NSIDC	3.50
CESM2	5.45
CESM2-WACCM	5.30
CESM2-WACCM-FV2	5.17
CMCC-CM2-SR5	6.78
CMCC-ESM2	7.10
E3SM-1-0	5.27
EC-Earth3	6.39
EC-Earth3-AerChem	6.35
EC-Earth3-CC	6.88
EC-Earth3-Veg	6.64
EC-Earth3P	5.38
HadGEM3-GC31-MM	4.77
MRI-ESM2-0	6.60
NorESM2-MM	5.76
SAM0-UNICON	5.15

Fig. 2. Boxplots comparing sea ice drift speeds between monthly NSIDC-Pathfinder data and fifteen CMIP6 models, based on all grid points (The upper and lower boundaries of the box represent the upper and lower quartiles of monthly sea ice drift speeds, respectively. Thick lines represent the medians of the monthly sea ice drift speeds, and the upper and lower lines represent the maximum and minimum values of monthly speeds, respectively. Triangles indicate average monthly sea ice drift speeds. Inset table displays corresponding average monthly sea ice drift speeds (km d^{-1})).

Table 2
1979−2014 mean of pan-Arctic averaged sea ice drift speed, sea ice area flux through the Fram Strait, and the maximum rotation in the Beaufort Gyre for NSIDC datasets and fifteen models.

Source	Pan-Arctic averaged sea ice drift speed (km d^{-1})	Sea ice area flux through the Fram Strait ($\times$ 10^6 km^2)	Maximum rotation in the Beaufort Gyre
NSIDC	3.51	0.58	0.83
CESM2	5.43	0.65	0.93
CESM2-WACCM	5.29	0.63	0.91
CESM2-WACCM-FV2	5.14	0.50	0.92
CMCC-CM2-SR5	6.62	0.27	0.87
CMCC-ESM2	6.93	0.31	0.91
E3SM-1-0	5.11	0.65	0.92
EC-Earth3	6.28	0.61	0.93
EC-Earth3-AerChem	6.23	0.68	0.95
EC-Earth3-CC	6.71	0.75	0.95
EC-Earth3-Veg	6.48	0.70	0.95
EC-Earth3P	5.24	0.70	0.88
HadGEM3-GC31-MM	4.76	0.80	0.87
MRI-ESM2-0	6.54	0.75	0.89
NorESM2-MM	5.69	0.83	0.90
SAM0-UNICON	5.03	0.77	0.88

observational data by 4%−14%). This indicates an overestimation of angle differences in sea ice drifts around the Beaufort Gyre's center. Additionally, the spatial pattern of sea ice drift near the rotation center is closer to a perfect circular shape than what is observed in NSIDC-Pathfinder. Two models (i.e., CMCC-CM2-SR5 and HadGEM3-GC31-MM) produce maximum rotation values relatively close to the NSIDC-Pathfinder value. Consequently, HadGEM3-GC31-MM exhibits good simulation performance for both pan-Arctic sea ice drift speed and sea ice drift angular differences around the Beaufort Gyre's center. EC-Earth3 displays a good representation of the sea ice area flux through the Fram Strait. However, the simulation performance for the Fram Strait sea ice area flux demonstrates notable differences from that of sea ice drift simulation, as the flux calculation uses both sea ice concentration and drift speed.

Fig. 3 shows the 1979−2014 averaged pan-Arctic sea ice drift speed for individual months, as derived from the NSIDC-

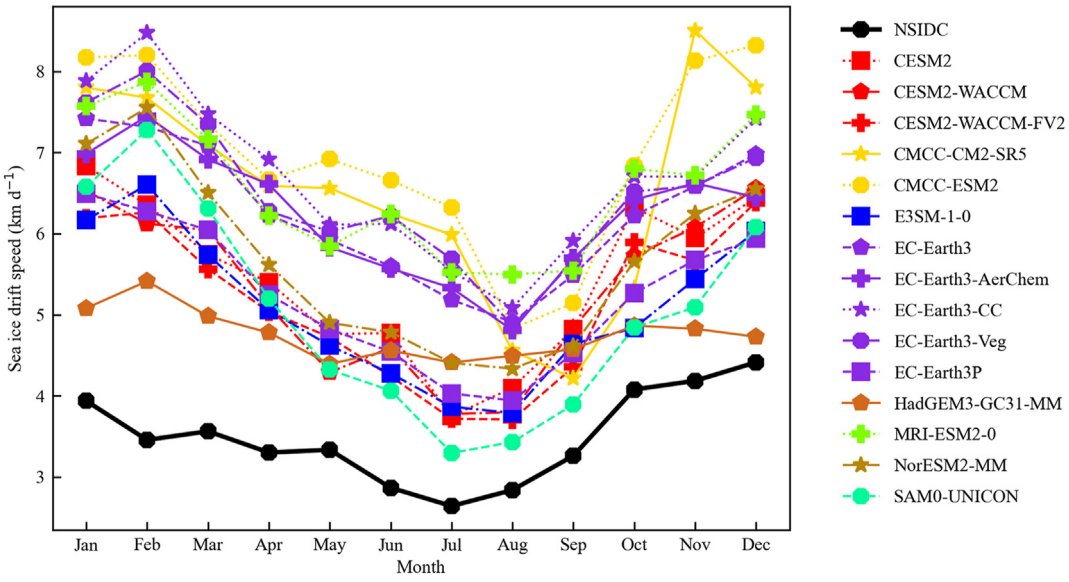

Fig. 3. Mean annual cycle of pan-Arctic sea ice drift speed for NSIDC-Pathfinder and fifteen models (1979−2014).

Table 3
Seasonal evolution of 1979−2014 averaged monthly pan-Arctic sea ice drift speed for NSIDC and fifteen models.

Source	Month with the minimum averaged sea ice drift speed	Month with the maximum averaged sea ice drift speed	Standard deviation of the averaged sea ice drift speed in 12 mon (km d^{-1})
NSIDC	July	December	0.54
CESM2	July	January	0.95
CESM2-WACCM	July	December	0.98
CESM2-WACCM-FV2	August	December	0.94
CMCC-CM2-SR5	September	November	1.28
CMCC-ESM2	August	December	1.11
E3SM-1-0	August	February	0.88
EC-Earth3	August	January	0.81
EC-Earth3-AerChem	August	February	0.74
EC-Earth3-CC	August	February	0.96
EC-Earth3-Veg	August	February	0.86
EC-Earth3P	August	January	0.83
HadGEM3-GC31-MM	May	February	0.29
MRI-ESM2-0	August	February	0.81
NorESM2-MM	August	February	1.05
SAM0-UNICON	July	February	1.24

pathfinder and fifteen models. Table 3 provides information on the months with minimum and maximum 1979−2014 averaged sea ice drift speeds, along with the standard deviation for 12 mon. As observed in Fig. 3, all models consistently overestimate the 1979−2014 averaged sea ice drift speed across all months. Nevertheless, the seasonal patterns of sea ice drift speed in all models resemble those in the NSIDC-pathfinder. Specifically, the maximum speed occurs in winter (December−February), followed by a gradual decline from spring (March−May) to summer (June−August), reaching its minimum speed in summer, and then gradually increasing again from summer to autumn (September−November) and back to winter each year. Table 3 reveals that only CESM2-WACCM displays minimum and maximum values coinciding with the same months as the NSIDC-Pathfinder. In comparison to the other models, HadGEM3-GC31-MM demonstrates the most significant discrepancy in the months exhibiting minimum and maximum values relative to the NSIDC-Pathfinder. The seasonal variability among the 12 mon, defined as the standard deviation of multi-year averaged monthly sea ice drift speed, is 0.54 km d^{-1} in the NSIDC-Pathfinder. Among all models, HadGEM3-GC31-MM displays smaller seasonal variability (0.29 km d^{-1}) than the NSIDC-Pathfinder, while the other fourteen models exhibit larger variability (0.74−1.28 km d^{-1}). The seasonal variability in EC-Earth3-AerChem (0.74 km d^{-1}) most closely aligns with that of the NSIDC-Pathfinder.

3.2. Trend of sea ice drift

Fig. 4 presents the time series and linear trends of annual pan-Arctic averaged sea ice drift speed for all models and the

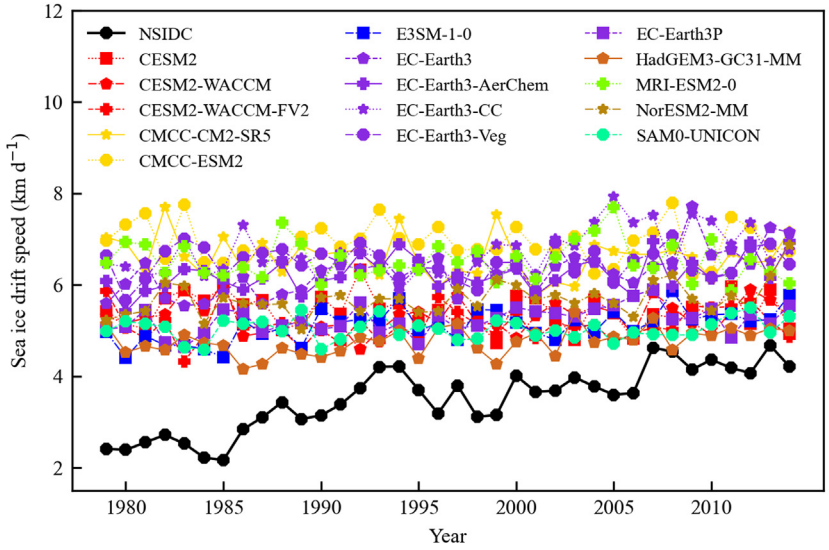

NSIDC	0.58*
CESM2	−0.05
CESM2-WACCM	0.06
CESM2-WACCM-FV2	0.03
CMCC-CM2-SR5	−0.07
CMCC-ESM2	−0.05
E3SM-1-0	0.20*
EC-Earth3	0.33*
EC-Earth3-AerChem	0.13*
EC-Earth3-CC	0.24*
EC-Earth3-Veg	0.01
EC-Earth3P	0.12*
HadGEM3-GC31-MM	0.11*
MRI-ESM2-0	−0.02
NorESM2-MM	0.15*
SAM0-UNICON	0.03

Fig. 4. Pan-Arctic averaged sea ice drift speed comparison between NSIDC-Pathfinder and fifteen models (1979−2014) (Inset table displays corresponding linear trends (km d^{-1} per decade). An asterisk indicates a trend with a confidence level reaching 95%).

NSIDC-pathfinder from 1979 to 2014. All fifteen models consistently overestimate sea ice drift speed across all years. The NSIDC-pathfinder exhibits a significant increasing trend of 0.58 km d^{-1} per decade. Among the models, seven (E3SM-1-0, EC-Earth3, EC-Earth3-AerChem, EC-Earth3-CC, EC-Earth3P, HadGEM3-GC31-MM, NorESM2-MM) display a significant increasing trend (0.11−0.33 km d^{-1} per decade, with EC-Earth3 exhibiting the strongest trend of the seven. However, EC-Earth3's trend of 0.33 km d^{-1} per decade remains weaker than that of the NSIDC. The remaining eight models do not demonstrate a significant trend.

Fig. A1 presents the time series and linear trends of annual sea ice area flux through the Fram Strait from 1979 to 2014. Between 1979 and 1987, the CMCC-CM2-SR5 and CMCC-ESM2 models simulate annual sea ice area fluxes through the Fram Strait that closely align with the fluxes derived from satellite-based datasets of NSIDC, while the other models tend to overestimate these fluxes. However, from 1987 to 2014, the CMCC-CM2-SR5 and CMCC-ESM2 models underestimate the annual sea ice area fluxes, whereas the other models exhibit greater agreement with the satellite-derived datasets. According to satellite-derived datasets, a significant increasing trend of 13.25×10^3 km^2 per year is observed in the sea ice area flux through the Fram Strait. Among all models, seven (i.e., E3SM-1-0, EC-Earth3, EC-Earth3-AerChem, EC-Earth3-CC, EC-Earth3P, HadGEM3-GC31-MM, and MRI-ESM2-0) display significant increasing trends ($(3.94-13.55) \times 10^3$ km^2 per year). Notably, the increasing trends of EC-Earth3 and EC-Earth3-AerChem, at 13.36×10^3 and 13.55×10^3 km^2 per year, respectively, closely match the trend calculated from satellite-derived datasets. The increase trends of the other five models (i.e., ESM-1-0, EC-Earth3-CC, EC-Earth3P, HadGEM3-GC31-MM, and MRI-ESM2-0) are weaker. EC-Earth3-Veg exhibits a significant decreasing trend (i.e., -3.24×10^3 km^2 per year). For the remaining seven models, no significant trend is detected in the sea ice area flux through the Fram Strait.

Fig. A2 presents the time series and linear trends of the annual maximum rotation in the Beaufort Gyre from 1979 to 2014. Over the years, the majority of models yield similar or slightly overestimated results for the annual maximum rotation in the Beaufort Gyre when compared to the data obtained from NSIDC-Pathfinder. Nonetheless, some models, specifically CMCC-CM2-SR5, CESM2, and SAM0-UNICON, demonstrate a significant underestimation in individual years. Fig. 5 illustrates the spatial distribution of sea ice drift and rotation as simulated by the models and NSIDC-Pathfinder during periods of considerable underestimation of the maximum rotation. The cases of overestimation during the same period are also presented in Fig. 5 for comparison. This comparison reveals that the models' inability to capture the Beaufort Gyre leads to an underestimation of the annual maximum rotation in the Beaufort Gyre. Additionally, the overestimation of that value shows a spatial pattern in sea ice drift near the rotation center that is more closely aligned with a perfectly circular shape than what is observed in NSIDC-Pathfinder. While NSIDC-Pathfinder's data on the annual maximum rotation in the Beaufort Gyre do not exhibit a significant trend, most models similarly do not show any significant trends. Only NorESM2-MM simulates a weak and significant increasing trend, whereas EC-Earth3-Veg and CMCC-CM2-SR5 simulate a weak but significant decreasing trend. Consequently, with the exception of CMCC-CM2-SR5, CESM2, and SAM0-UNICON, the remaining 12 models provide a reasonably accurate representation of the Beaufort Gyre.

4. Influence of near-surface wind and surface ocean current on model simulations

4.1. Dependency of sea ice drift on near-surface wind and surface ocean current

Fig. A3 displays scatter plots comparing near-surface wind speed and sea ice drift speed for each model and observation/

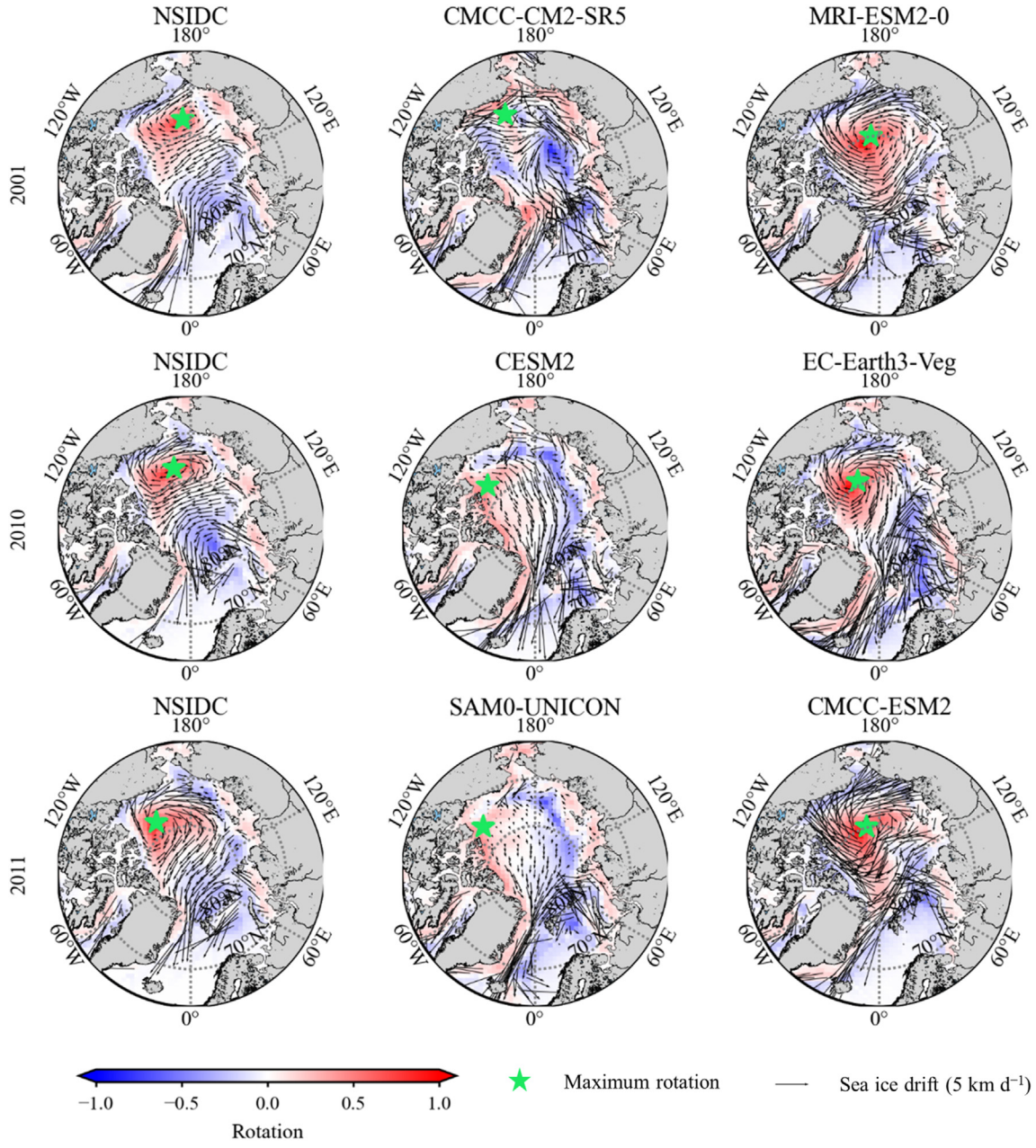

Fig. 5. Spatial distribution of sea ice drift and rotation derived from NSIDC-Pathfinder and models during years with notable rotation underestimation (The second column shows the underestimation cases. The third column exhibits the overestimation cases during the same period for comparison).

reanalysis data. Near-surface wind speed is divided into six intervals, with each interval spanning 2 m s^{-1}. The relationship between the sea ice drift speed from NSIDC and near-surface wind speed from ERA5 exhibits a strong and positive correlation (0.989). All models effectively simulate the positive correlation between sea ice drift speed and near-surface wind speed, yielding correlation coefficients ranging from 0.987 to 0.999, with no noticeable differences among them. When near-surface wind speed exceeds 3 m s^{-1}, all simulation models overestimate the sea ice drift speed compared to observational data. However, under low wind speed conditions (below 3 m s^{-1}), the model-simulated sea ice drift speed shows good agreement with the observed data. Additionally, the linear slopes of the simulated data in these models are notably higher than the slope derived from the observation/reanalysis data (0.843). The above findings suggest a greater influence of simulated near-surface wind speed on sea ice drift speed within the models compared to observation/reanalysis data. Among the models, NorESM2-MM shows the highest slope value of 2.250, while CESM2-WACCM-FV2 exhibits the lowest slope value of 1.195.

Fig. A4 presents scatter plots comparing surface ocean current speed and sea ice drift speed for each model and observation/reanalysis data. Surface ocean current speed is divided into six intervals, with each interval spanning 2 cm s^{-1}. The sea ice drift speed from NSIDC and surface

ocean current speed from ORAS5 display a strong positive correlation, yielding a correlation coefficient of 0.997. All models successfully capture the positive correlation between sea ice drift speed and surface ocean current speed, with correlation coefficients ranging from 0.993 to 1.000 and negligible differences among them. The majority of simulation models overestimate the sea ice drift speed compared to observational data under the same surface ocean current speed. Only a few models show a slight underestimation of sea ice drift speed at low surface ocean current speeds (around 1 cm s^{-1}). In contrast to the slope value of 0.312 derived from observation/reanalysis data, MRI-ESM2-0 exhibits the highest slope value of 1.391, while EC-Earth3P demonstrates the lowest slope value of 0.895. The findings suggest a more pronounced impact of simulated surface ocean current speed on sea ice drift speed within the models relative to observation/reanalysis data.

4.2. Mean bias associated with near-surface wind and surface ocean current

Fig. 6 displays boxplots of near-surface wind speeds and surface ocean current speeds derived from monthly reanalysis data and fifteen CMIP6 models, based on all grid points. Fig. 6a shows that all models simulate near-surface wind speeds with similar mean, median, lower quartile, and upper quartile values, all of which are higher than those in ERA5. Fig. 6b demonstrates that CESM2, CESM2-WACCM, CESM2-WACCM-FV2, and SAM0-UNICON exhibit surface ocean current speeds similar to ORAS5 in terms of mean, median, lower quartile, and upper quartile values. E3SM-1-0, HadGEM3-GC3-MM, and MRI-ESM2-0 display median and lower quartile values resembling ORAS5, though their mean and upper quartile values are overestimated. The remaining eight models present results exceeding ORAS5 across mean, median, lower quartile, and upper quartile values. Consequently, it can be inferred that while all models overestimate monthly-averaged near-surface wind speeds, their performance in simulating monthly-averaged surface ocean current speeds is variable. This suggests that the overestimation of monthly sea ice drift speed in the models may be primarily attributed to the overestimation of monthly near-surface wind speeds.

Table 4 displays the 1979−2014 mean of pan-Arctic averaged near-surface wind speed and surface ocean current speed. All models overestimate the 1979−2014 mean of pan-Arctic averaged near-surface wind speed relative to ERA5 (2.38 m s^{-1}), with simulated values ranging from 3.19 to 3.60 m s^{-1} (exceeding the reanalysis data by 34%−51%). CESM2, CESM2-WACCM, and CESM2-WACCM-FV2 slightly underestimate the 1979−2014 mean of pan-Arctic averaged surface ocean current speed compared to ORAS5 (3.03 cm s^{-1}), with simulated values ranging from 2.83 to 2.99 cm s^{-1} (1%−6% below the reanalysis data), while the remaining 12 models overestimate it, with values ranging from 3.15 to 4.76 cm s^{-1} (exceeding the reanalysis data by 4%−57%). Eight models (CMCC-CM2-SR5, CMCC-ESM2, EC-Earth3, EC-Earth3-AerChem, EC-Earth3-CC, EC-Earth3P, EC-Earth3-Veg, NorESM2-MM) show a value that exceeds the reanalysis data by more than 28%. The above findings demonstrate that sea ice drift speed in all fifteen models is notably overestimated, as is the near-surface wind speed in all models. However, among the fifteen models, not all show a marked overestimation of surface ocean current speed, and some even slightly underestimate that speed. Furthermore, Fig. A3

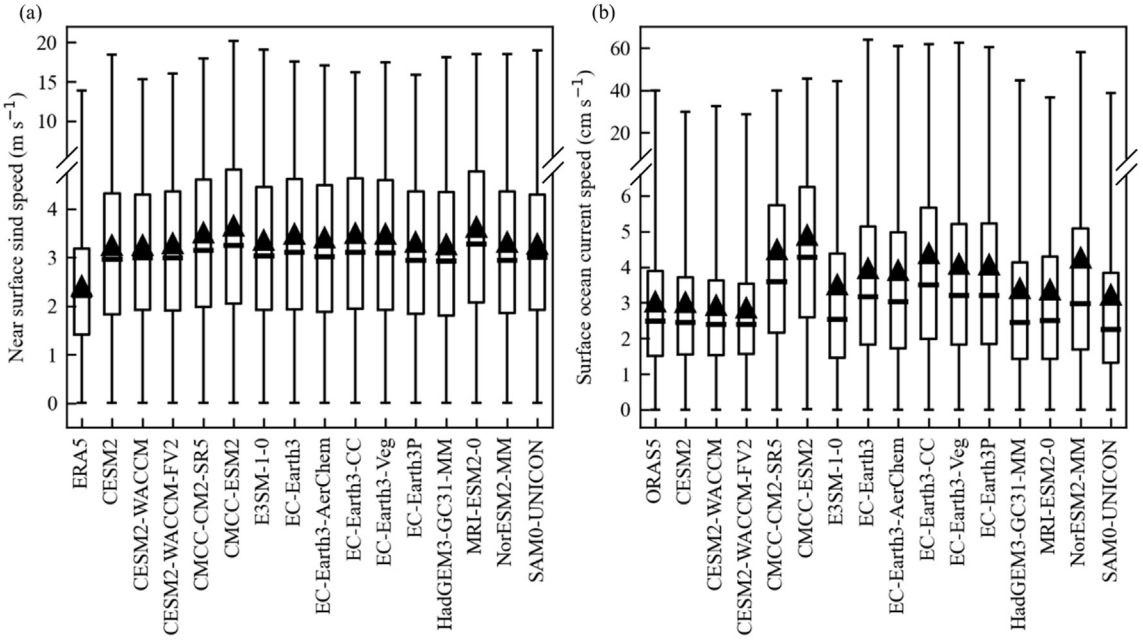

Fig. 6. Boxplots comparing near-surface wind speeds (a) and surface ocean current speeds (b) between ERA5/ORAS5 data and fifteen CMIP6 models, based on all grid points (The upper and lower boundaries of the box represent the upper and lower quartile values, respectively. Thick lines represent the medians, and the upper and lower lines represent the maximum and minimum values, respectively. Triangles indicate mean values).

Table 4
1979−2014 mean of pan-Arctic averaged near-surface wind speed and surface ocean current speed for reanalysis datasets and fifteen models.

Source	Pan-Arctic averaged near-surface wind speed (m s^{-1})	Pan-Arctic averaged surface ocean current speed (cm s^{-1})
ERA5/ORAS5	2.38	3.03
CESM2	3.23	2.99
CESM2-WACCM	3.23	2.90
CESM2-WACCM-FV2	3.25	2.83
CMCC-CM2-SR5	3.32	4.25
CMCC-ESM2	3.50	4.76
E3SM-1-0	3.26	3.36
EC-Earth3	3.36	3.97
EC-Earth3-AerChem	3.29	3.88
EC-Earth3-CC	3.35	4.35
EC-Earth3P	3.33	4.04
EC-Earth3-Veg	3.19	4.01
HadGEM3-GC31-MM	3.23	3.39
MRI-ESM2-0	3.60	3.35
NorESM2-MM	3.25	4.20
SAM0-UNICON	3.32	3.15

suggests that the simulated near-surface wind speed has a greater impact on sea ice drift speed within the models than observation or reanalysis data. Therefore, the overestimation of both the near-surface wind speed and its influence on sea ice drift speed may be the primary factors contributing to the overestimation of sea ice drift speed within these models.

Fig. 7 shows the 1979−2014 averaged pan-Arctic near-surface wind speed and surface ocean current speed for individual months, as derived from the reanalysis datasets and fifteen models. Table 5 provides information on the months with minimum and maximum 1979−2014 averaged near-surface wind speeds and surface ocean current speeds, along with the standard deviation for 12 mon. Fig. 7a illustrates that nearly all models have higher 1979−2014 averaged near-surface wind speeds than ERA5 across all months. As shown in Table 5, ERA5's near-surface wind speed attains its minimum in July and maximum in January. Among the models, only CESM2 shares the same months for maximum and minimum values with ERA5. Most of the other models exhibit minimum values in July or August and maximum values in January or February, with the exception of CMCC-CM2-SR5 and CESM2-WACCM, which display their minimum in October and maximum in March, respectively. In terms of the seasonal variability of near-surface wind speed, ERA5 obtains a value of 0.34 m s^{-1}, whereas all models present overestimated simulations ranging from 0.42 to 0.74 m s^{-1}.

For the 1979−2014 averaged surface ocean current speed, CESM2, CESM2-WACCM, CESM2-WACCM-FV2, E3SM-1-0, and SAM0-UNICON generally exhibit lower values than ORAS5 during the sea ice melting season (May−September) and higher values during the freezing season (October−April), while the remaining ten models display higher values than ORAS5 for all months (Fig. 7b). As shown in Table 5, ORAS5's surface ocean current speed reaches its minimum in October and maximum in June, with only CMCC-CM2-SR2 sharing these months for maximum and minimum values. The seasonal variability of ORAS5's surface ocean current speed is 0.25 cm s^{-1}, which is correctly simulated by CESM2, CESM2-WACCM, and EC-Earth3-Veg, while CESM2-WACCM-FV2, EC-Earth3, EC-Earth3-AerChem, and MRI-ESM2-0 exhibit slightly lower variabilities (0.21−0.24 cm s^{-1}) and HadGEM3-GC31-MM displays a notably lower variability (0.17 cm s^{-1}) compared to ORAS5. The remaining seven models overestimate seasonal variability.

A comparison of Figs. 3 and 7 and Tables 3 and 5 reveals that in observation/reanalysis data, the seasonal evolution of sea ice drift aligns with the seasonal variations in near-surface wind speed but not with the corresponding changes in surface ocean current speed. Almost all models simulate this consistency between sea ice drift and near-surface wind speed seasonal evolution, with only CMCC-CM2-SR2, CMCC-ESM2, HadGEM3-GC31-MM, and MRI-ESM2-0 reflecting the inconsistency between sea ice drift and surface ocean current

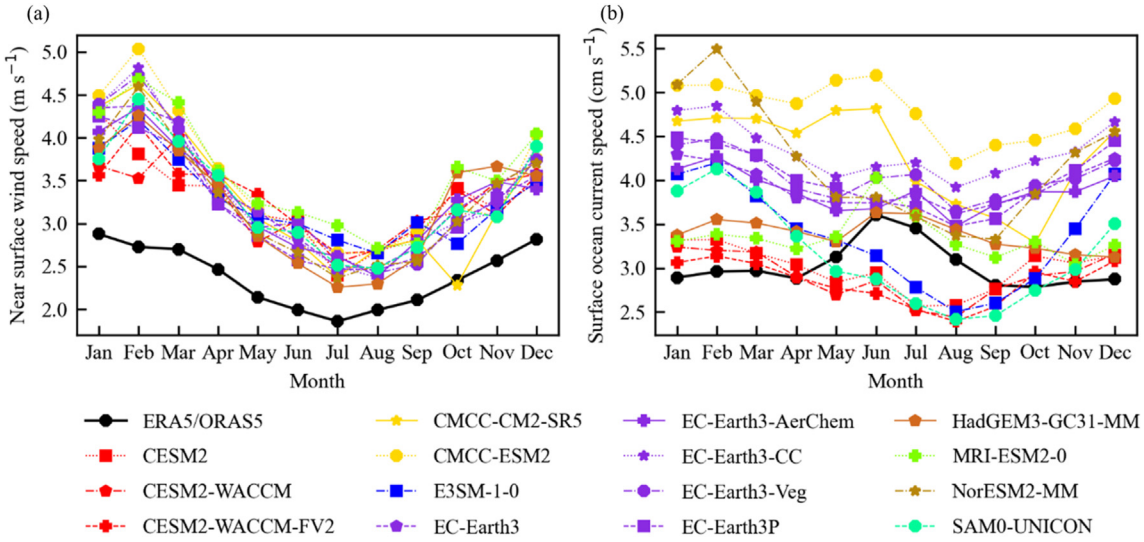

Fig. 7. Mean annual cycle of pan-Arctic near-surface wind speed (a) and surface ocean current speed (b) based on reanalysis data and fifteen models (1979−2014).

Table 5
Seasonal evolution of 1979–2014 averaged monthly pan-Arctic near-surface wind speed and surface ocean current speed for reanalysis data and fifteen models.

Source	Near-surface wind speed			Surface ocean current speed		
	Month with the minimum value	Month with the maximum value	Standard deviation (m s^{-1})	Month with the minimum value	Month with the maximum value	Standard deviation (cm s^{-1})
ERA5/ORAS5	July	January	0.34	October	June	0.25
CESM2	July	January	0.49	July	February	0.25
CESM2-WACCM	July	March	0.42	August	January	0.25
CESM2-WACCM-FV2	July	February	0.42	August	February	0.23
CMCC-CM2-SR5	October	February	0.75	October	June	0.51
CMCC-ESM2	August	February	0.76	August	June	0.31
E3SM-1-0	August	February	0.46	August	February	0.57
EC-Earth3	August	February	0.65	August	January	0.22
EC-Earth3-AerChem	August	February	0.59	August	February	0.21
EC-Earth3-CC	August	February	0.75	August	February	0.29
EC-Earth3-Veg	August	February	0.72	August	February	0.25
EC-Earth3P	August	January	0.62	August	January	0.33
HadGEM3-GC31-MM	July	February	0.66	December	June	0.17
MRI-ESM2-0	August	February	0.63	November	June	0.24
NorESM2-MM	July	February	0.67	September	February	0.67
SAM0-UNICON	August	February	0.60	August	February	0.56

speed seasonal evolution. Furthermore, the overestimation of near-surface wind speed's seasonal variability by the models may primarily account for the overestimated seasonal variability of sea ice drift.

4.3. Trend bias associated with near-surface wind and surface ocean current

Fig. 8 displays the time series and linear trends of annual pan-Arctic averaged near-surface wind speed for all models and ERA5 from 1979 to 2014. The near-surface wind speed is overestimated by all models in every year, which may be a crucial factor for the overestimation of sea ice drift speed across all years. In ERA5, the near-surface wind speed exhibits no significant trend, suggesting that the significant increase in sea ice drift speed is not attributed to an increasing trend in near-surface wind speed. This conclusion aligns with findings from previous studies. Spreen et al. (2011) reported that the changes in wind speed account for a portion of the observed drift speed increase in the Central Arctic but not the entire basin during 1992–2009. Rampal et al. (2009) suggested that the increase in sea ice mean speed is unlikely due to stronger wind forcing. Among the models, CESM2-WACCM-FV2 and EC-Earth3P display a weak and significant decreasing trend, while E3SM-1-0 shows a weak and significant increasing trend. The remaining twelve models exhibit no significant trend. Consequently, nearly all models capture the non-significant trend of near-surface wind speed. Thus, the absence of a significant increasing trend in sea ice drift simulation by the models is not attributable to their failure to simulate the near-surface wind speed trend.

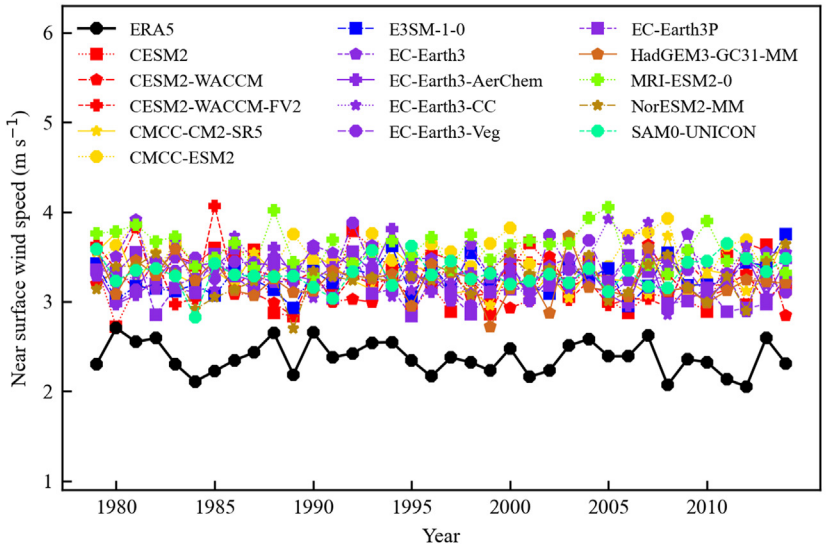

ERA5	−0.04
CESM2	−0.04
CESM2-WACCM	−0.02
CESM2-WACCM-FV2	−0.06*
CMCC-CM2-SR5	−0.04
CMCC-ESM2	−0.02
E3SM-1-0	0.06*
EC-Earth3	−0.03
EC-Earth3-AerChem	−0.03
EC-Earth3-CC	0.03
EC-Earth3-Veg	−0.01
EC-Earth3P	−0.06*
HadGEM3-GC31-MM	−0.05
MRI-ESM2-0	−0.04
NorESM2-MM	0.02
SAM0-UNICON	0.03

Fig. 8. Pan-Arctic averaged near-surface wind speed comparison between ERA5 and fifteen models (1979–2014) (Inset table displays corresponding linear trends (m s^{-1} per decade). An asterisk indicates a trend with a confidence level reaching 95%).

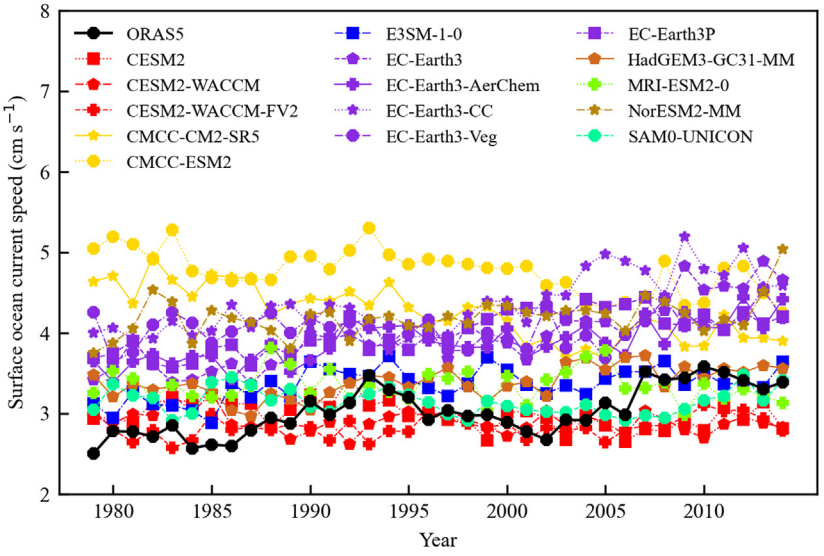

ORAS5	0.21*
CESM2	−0.07*
CESM2-WACCM	−0.04
CESM2-WACCM-FV2	0.04*
CMCC-CM2-SR5	−0.26*
CMCC-ESM2	−0.17*
E3SM-1-0	0.10*
EC-Earth3	0.33*
EC-Earth3-AerChem	0.18*
EC-Earth3-CC	0.26*
EC-Earth3-Veg	0.04
EC-Earth3P	0.19*
HadGEM3-GC31-MM	0.11*
MRI-ESM2-0	−0.02
NorESM2-MM	0.10*
SAM0-UNICON	−0.02

Fig. 9. Pan-Arctic averaged surface ocean current speed comparison between ORAS5 and fifteen models (1979–2014) (Inset table displays corresponding linear trends (cm s^{-1} per decade). An asterisk indicates a trend with a confidence level reaching 95%).

Fig. 9 presents the time series and linear trends of annual pan-Arctic averaged surface ocean current speed for all models and ORAS5 from 1979 to 2014. Models within the same family produce similar results in surface ocean current speed simulations, while those from different model families exhibit notable differences. Furthermore, the CMCC and EC families, which use the NEMO3.6 ocean model, consistently produce higher surface ocean current speeds than the reanalysis data. However, the models of the CESM2 family and SAM0-UNICON, which use the POP2 ocean model, exhibit consistent results that align with the reanalysis data. Although other models use different ocean models, their results are also consistent with the reanalysis data. The findings suggest that the choice of ocean model can substantially impact surface ocean current speed simulations. In particular, our results suggest that using NEMO3.6 ocean models may not be the optimal choice when compared to other ocean models listed in Table A1. As not all models consistently overestimate surface ocean current speed, it is unlikely to be the primary cause of sea ice drift speed overestimation in all years. ORAS5 reveals a significant increasing trend in surface ocean current speed at 0.21 cm s^{-1} per decade. Among the models, eight (CESM2-WACCM-FV2, E3SM-1-0, EC-Earth3, EC-Earth3-AerChem, EC-Earth3-CC, EC-Earth3P, HadGEM3-GC31-MM, and NorESM2-MM) exhibit a significant increasing trend, while CESM2, CMCC-CM2-SR5, and CMCC-ESM2 display a significant decreasing trend. The remaining four models demonstrate no significant trend. Among the eight models exhibiting significant increasing trends, CESM2-WACCM-FV2 displays the weakest trend at only 0.04 cm s^{-1} per decade, while the other seven models exhibit trends ranging from 0.10 to 0.33 cm s^{-1} per decade. These seven models are the ones that simulate increasing trends in sea ice drift velocity. Consequently, an inability to simulate an increasing trend in surface ocean current speed might be a reason for the models' failure to reproduce the sea ice drift velocity trend.

5. Discussion

The results presented above show that the simulated sea ice drift speed is higher than that of the observed data, and it is suggested that the overestimation of near-surface wind speed in the models may potentially be linked to the overestimation of sea ice drift speed. As the influence of wind on sea ice varies with its thickness, this study further examined the relationship between sea ice drift speed, sea ice thickness, and near-surface wind speed. Sea ice thickness data used for evaluation were from the Pan-Arctic Ice Ocean Modeling and Assimilation System (PIOMAS), which was developed by the University of Washington (Zhang and Rothrock, 2003). Numerous studies have verified the reliability of the PIOMAS sea ice thickness data (Laxon et al., 2013; Schweiger et al., 2011; Stroeve et al., 2014). Fig. 10 illustrates the average sea ice drift speed and near-surface wind speed across different sea ice thickness classes, derived from monthly NSIDC-Pathfinder, PIOMAS thickness, ERA5 data, and fifteen CMIP6 models at all grid cells. Sea ice thickness is divided into five intervals, with each interval spanning 1 m. The NSIDC-pathfinder/POIMAS data reveal a decrease in sea ice drift speed with an increase in sea ice thickness. This relationship is accurately captured by all models except EC-Earth3P. However, it is noted that within each sea ice thickness class, the models report higher sea ice drift speeds and near-surface wind speeds compared to observational/reanalysis data. This suggests that the overestimation of sea ice drift speeds in the models appears to primarily result from the overestimation of near-surface wind speed.

As the pressure gradient force drives the wind, this study further analyzed the relationship between simulated sea level pressure and sea ice drift. Monthly sea level pressure data from ERA5 were used for evaluation, while EC-Earth3P and HadGEM3-GC31-MM were excluded from the analysis due to the unavailability of monthly sea level pressure simulation

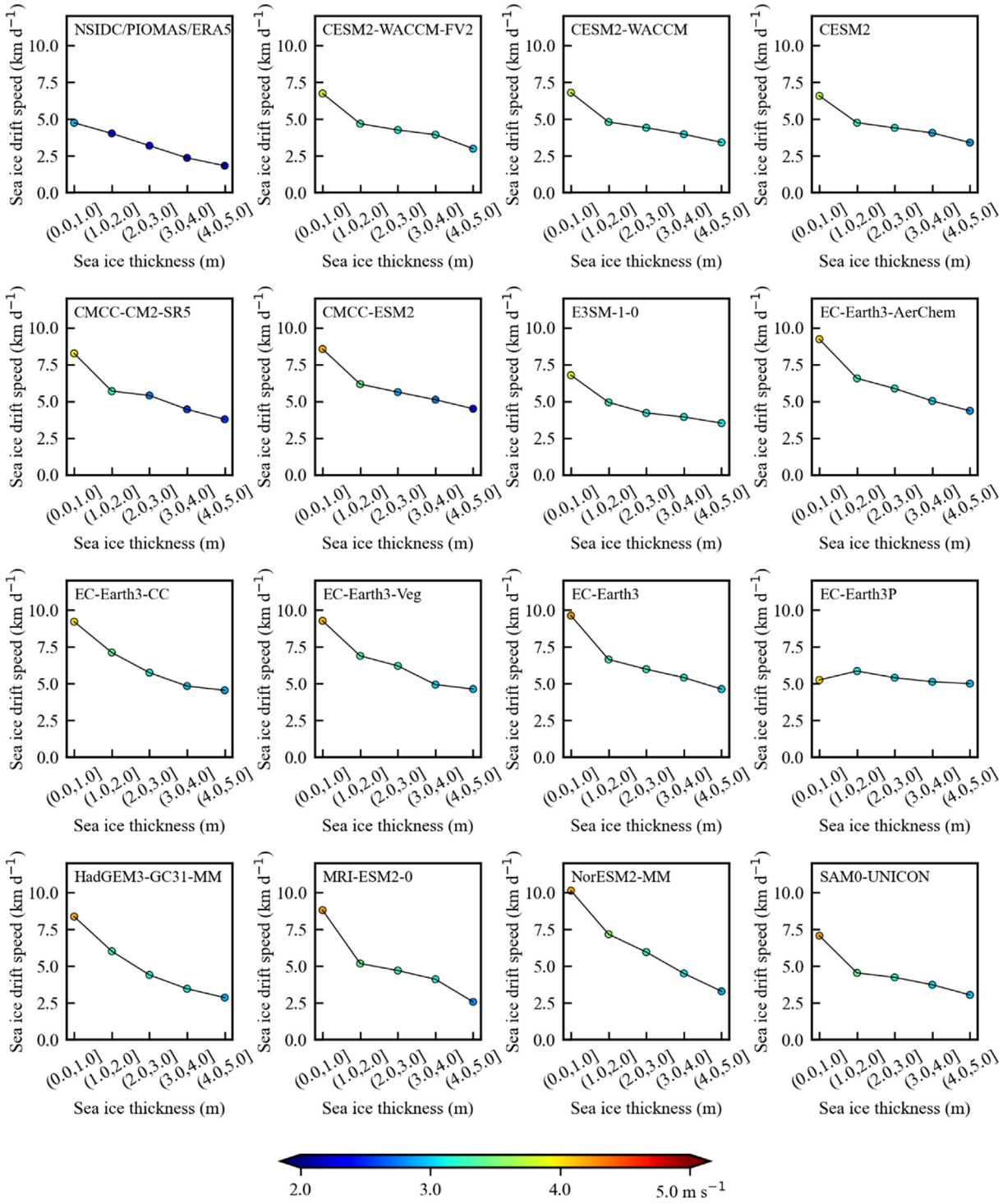

Fig. 10. Relationship between sea ice drift speed and sea ice thickness across all grid points for monthly observational/reanalysis data and fifteen models (The *y*-axis values of the dots represent the average sea ice drift speed, while their colors indicate the average near-surface wind speed).

results. Fig. A5 presents the spatial distribution of mean sea ice drift, rotation, and sea level pressure for 1979−2014, derived from monthly NSIDC-Pathfinder, ERA5 data, and thirteen CMIP6 models. The figure shows that there is minimal difference in pressure gradient between the reanalysis data and the model simulations, indicating that the overestimation of near-surface wind speed in sea ice regions may not be due to biases in the pressure gradient simulated by the model. Instead, biases in parameterizations of sea ice−atmosphere interactions and sea ice conditions (i.e. sea ice concentration and thickness) could lead to the overestimation of near-surface wind speed, which remains to be investigated in the future. In addition, Fig. A5 shows that among the thirteen models, the CMCC-CM2-SR5 and CMCC-ESM2 models exhibit significant differences in the

direction of simulated pressure gradients compared to the reanalysis data, particularly in the regions of transpolar drift and Kara/Barents Seas. As a consequence, these models display considerable biases in the speed and direction of sea ice drift in these regions when compared to the observational data. This finding partially explains why these two models display a larger MAE in sea ice drift speed compared to the other models (as shown in Table 1).

Furthermore, in the observational/reanalysis data, the position of Beaufort High is found to be in good agreement with the sea ice circulation around the Beaufort Gyre, and the center of the Beaufort High, which corresponds to the location of its maximum pressure, is closely aligned with the position of maximum rotation of sea ice drift. CESM2-WACCM-FV2, E3SM-1-0, EC-Earth3, EC-Earth3-Aerchem, EC-Earth3-CC, and EC-Earth3-Veg models perform well in simulating this alignment, indicating their ability to capture the relationship between the Beaufort High and sea ice circulation around the Beaufort Gyre. However, reanalysis data shows the center of the Beaufort High to be located in the Beaufort Sea, while the models exhibit some offset, closer to the central Arctic. Moreover, these models show some differences in the strength of Beaufort High when compared to the reanalysis data. Consequently, these models exhibit biases in the sea ice drift speed and the position of sea ice circulation in the Beaufort Gyre, as well as in the location of the maximum rotation of sea ice drift, when compared to the observational data.

In addition to the analysis of the relationship between simulated mean sea level pressure and sea ice drift, this study also investigated the influence of major high-latitude circulation patterns on sea ice drift simulations. Arctic Oscillation (AO) and Arctic Dipole (AD) are the two dominant patterns of Arctic atmospheric circulation (Zhang et al., 2021). The cyclonic circulations of ice motion are mainly associated with the AO (Kwok et al., 2013; Rigor et al., 2002), while AD affects the sea ice motion along the Transpolar Drift Stream (Dethloff et al., 2022; Wu et al., 2006; Zhang et al., 2021). In this study, empirical orthogonal function (EOF) analysis was carried out to obtain the leading modes of atmospheric variability in sea level pressure over the Arctic region (70°−90°N) during summer (June−August), winter (December−February), and the entire year. The first and second modes (EOF1 and EOF2) represent the AO and AD, respectively (Watanabe et al., 2006; Wu et al., 2006). The results show that most models capture the spatial patterns of AO and AD effectively in both summer and winter (Figs. A6−A9). However, CMCC-CM2-SR5 and EC-Earth3-Veg models fail to identify the dipole structure in EOF2 mode during winter and instead find it in EOF3 mode. Moreover, the direction of the zero isolines simulated by these two models is inconsistent with that in the reanalysis. Previous studies have shown that the AO index is related to the zonal sea ice drift speed, while the AD index is related to the meridional sea ice drift speed (Lei et al., 2016; Li et al., 2022; Zhang et al., 2021). Our analysis confirms this relationship (Tables A2−A3). The reanalysis data show that the correlation between the AO index and zonal sea ice drift speed is positive in both summer and winter, with a stronger correlation in summer, while the AD index is positively correlated with meridional sea ice drift speed, with a slightly stronger correlation in summer. Most models effectively capture this positive correlation. Moreover, in summer, most models simulate a higher positive correlation between the AO index and zonal meridional speed than in winter, and a higher positive correlation between the AD index and meridional speed than in winter, except for a few models. Based on the reanalysis data, the AO index does not display a significant trend in any season, which is consistent with the majority of models (Fig. A10 and Table A4). While the AD index exhibits a slight decreasing trend in winter according to the reanalysis data, it generally fluctuates around the neutral phase and may have minimal impact on the trend of transpolar drift. In summer, however, the AD index shows an increasing trend and shifts from a negative phase (indicating a slowdown in the transpolar drift) to a positive phase (indicating an acceleration of the transpolar drift), potentially contributing to the observed increase in sea ice drift speed and sea ice area flux through the Fram Strait (Figs. 3 and 4). Most models fail to reproduce the increasing trend of the AD index in summer, which may lead to biases in the trends of sea ice drift speed and sea ice area flux through the Fram Strait when compared to observational data. However, despite these limitations, some of these models successfully capture an increase in sea ice drift velocity and sea ice area flux through the Fram Strait. As such, further in-depth analyses are needed in the future to identify the possible linkages between the simulated AD index and the trends in sea ice drift speed and sea ice area flux through the Fram Strait. Nonetheless, since models that simulate an increasing trend in surface ocean current speed also simulate an increasing trend in sea ice drift (Figs. 4 and 9), one of the primary reasons for not reproducing an increasing trend in sea ice drift speed may be the failure to simulate a trend in surface ocean current speed. Moreover, data assimilation has not been implemented in the CMIP6 model results, potentially leading to some models failing to simulate the upward trend of sea ice drift speed and sea ice area flux through the Fram Strait. Additionally, Rampal et al. (2009) previously highlighted that changes in sea ice cover predominantly influence observed sea ice drift trends. Future research could focus on examining the influence of changes in sea ice conditions on the simulation of sea ice drift velocity trends.

Previous discussion explores potential explanations for the biases between the model simulations and the observation/reanalysis data. Furthermore, differences in the simulated sea ice drift speed and angle are observed among various models. Tables 1 and 2 present the performance of fifteen models, with HadGEM3-GC31-MM demonstrating relatively favorable results in terms of both the 1979−2014 average of pan-Arctic sea ice drift speed and the MAEs of sea ice drift speed and angle. The simulated 1979−2014 average of pan-Arctic sea ice drift speed by HadGEM3-GC31-MM (4.76 km d^{-1}) closely approximates the observed value of 3.51 km d^{-1}, and it exhibits the second lowest errors for speed, with an ME of 0.50 km d^{-1} and an MAE of 2.49 km d^{-1}, comparable to the lowest ME and MAE values of 0.48 km d^{-1} and 2.45 km d^{-1}, respectively. In addition, it achieves the lowest MAE for angle

(i.e., 67.09°). This may be attributed to the utilization of higher-resolution ocean and sea ice models in HadGEM3-GC31-MM (as shown in Table A1). Moreover, differences in sea ice drift simulation within the same family of models may arise from variations in model configurations. For example, within the CESM family, CESM2-WACCM exhibits better performance in sea ice drift simulation than CESM2, with its 1979−2014 average of pan-Arctic sea ice drift speed being closer to the observed value, and lower MAEs for sea ice drift speed and angle (as shown in Tables 1 and 2). A comparison of the model configurations (as shown in Table A1) reveals that CESM2-WACCM employs an atmosphere model with 70 vertical levels, and its model top is at 4.5×10^{-6} hPa. In contrast, CESM2's atmosphere model consists of 32 layers, with a model top at 2.26 hPa. CESM2-WACCM's atmosphere model, known as a 'high-top' model, possesses a superior representation of the stratosphere (Danabasoglu et al., 2020). Consequently, the 'high-top' atmosphere model may contribute to the enhanced accuracy of sea ice drift simulation. In the EC-Earth3 family, it is observed that EC-Earth3-AerChem demonstrates superior performance compared to EC-Earth3 in terms of the 1979−2014 average of pan-Arctic sea ice drift speed, as well as the MAEs for sea ice drift speed and angle. EC-Earth3-AerChem, which is the configuration with interactive aerosols and atmospheric chemistry utilized in the Aerosol and Chemistry Model Intercomparison Project (Döscher et al., 2022), demonstrates the potential benefits of including interactive aerosols and atmospheric chemistry in the atmosphere model for simulating sea ice drift.

The simulated Arctic sea ice drift was assessed against NSIDC-pathfinder data in this study. However, errors within the NSIDC Pathfinder product may introduce uncertainties in the validation results presented. Furthermore, this study only analyzed the influence of near-surface wind and surface ocean current on model simulations. Future research could investigate the influence of sea ice conditions on the simulation of sea ice drift velocity to further explain the discrepancies between simulated and observed sea ice drift. Additionally, examining model parameters that play key roles in determining climatological sea ice drift speed can help understand the spatiotemporal discrepancies in simulated sea ice drift of different models.

6. Conclusions

CMIP6 models are capable of replicating several aspects of the observed Arctic sea ice drift climatology and variability. They exhibit similar seasonal patterns of sea ice drift speed to the NSIDC-Pathfinder data and replicate the consistency between the seasonal patterns of sea ice drift and near-surface wind speed. Moreover, the models effectively reproduce the maximum rotation in the Beaufort Gyre. However, notable biases are identified. The models overestimate sea ice drift speed, with 1979−2014 mean drift speeds ranging from 4.76 to 6.93 km d^{-1}, compared to the observed speed of 3.51 km d^{-1}. Fourteen out of fifteen models display larger seasonal variability in sea ice drift (0.74−1.28 km d^{-1}) compared to observations (0.54 km d^{-1}). Seven models exhibit a significant increasing trend in sea ice drift (0.11−0.33 km d^{-1} per decade), but weaker than the NSIDC-Pathfinder (0.58 km d^{-1} per decade). The other eight models show no statistically significant trend. Discrepancies are also observed in the 1979−2014 mean of sea ice area flux through the Fram Strait, with models estimating a range of (0.27−0.80) $\times$ 10^6 km^2, while observations indicate 0.58×10^6 km^2.

To understand the causes of such biases, potential factors are explored. 1) An overestimation of both the near-surface wind speed and its impact on sea ice drift speed may be the primary factors contributing to the overestimation of sea ice drift speed within these models. 2) The models' overestimation of seasonal variability in near-surface wind speeds may play a key role in accounting for the overestimation of seasonal variability in sea ice drift. 3) A failure to simulate an increasing trend in surface ocean current speed may contribute to the models' inability to reproduce the sea ice drift velocity trend. It suggests that the utilization of higher-resolution ocean and sea ice models, the incorporation of a high-top atmospheric model, as well as the inclusion of interactive aerosols and atmospheric chemistry in the atmosphere model may improve the performance of Arctic sea ice drift simulation.

Declaration of competing interest

The authors declare no conflict of interest.

Acknowledgments

We greatly thank the Earth System Grid Federation (ESGF) for providing CMIP6 data (https://esgf-node.llnl.gov/search/cmip6/). We also thank NSIDC for providing NSIDC-Pathfinder (https://daacdata.app.nsidc.org/pub/DATASETS/nsidc0116_icemotion_vectors_v4/) and NSIDC-SIC (https://n5eil01u.ecs.nsidc.org/PM/NSIDC-0079.003/), ECMWF for providing ERA5 (https://cds.climate.copernicus.eu/cdsapp#!/dataset/reanalysis-era5-single-levels-monthly-means?tab=form) and ORAS5 (https://cds.climate.copernicus.eu/cdsapp#!/dataset/reanalysis-oras5?tab=form), and the University of Washington for providing PIOMAS (http://psc.apl.uw.edu/research/projects/arctic-sea-ice-volume-anomaly/data/).

We truly appreciate reviewers and editors for their constructive comments and suggestions, which greatly improved the quality of the manuscript. This research was funded by the National Key Research and Development Program of China (2021YFC2800705), the National Natural Science Foundation of China (42206247), Guangdong Basic and Applied Basic Research Foundation (2021A1515110779), and Fengyun Application Pioneering Project (FY-APP-2022.0201).

Appendix A. Supplementary data

Supplementary data to this article can be found online at https://doi.org/10.1016/j.accre.2023.09.005.

References

Colony, R., Thorndike, A.S., 1984. An estimate of the mean field of Arctic sea ice motion. J. Geophys. Res. 89, 10623. https://doi.org/10.1029/JC089iC06p10623.

Danabasoglu, G., Lamarque, J.F., Bacmeister, J., et al., 2020. The community Earth system model version 2 (CESM2). J. Adv. Model. Earth Syst. 12, e2019MS001916. https://doi.org/10.1029/2019MS001916.

de Vernal, A., Hillaire-Marcel, C., Le Duc, C., et al., 2020. Natural variability of the Arctic Ocean sea ice during the present interglacial. Proc. Natl. Acad. Sci. USA 117, 26069−26075. https://doi.org/10.1073/pnas.2008996117.

Derksen, C., Smith, S.L., Sharp, M., et al., 2012. Variability and change in the Canadian cryosphere. Clim. Change 115, 59−88. https://doi.org/10.1007/s10584-012-0470-0.

Dethloff, K., Maslowski, W., Hendricks, S., et al., 2022. Arctic sea ice anomalies during the MOSAiC winter 2019/20. Cryosphere 16, 981−1005. https://doi.org/10.5194/tc-16-981-2022.

Dewey, S., Morison, J., Kwok, R., et al., 2018. Arctic ice−ocean coupling and Gyre equilibration observed with remote sensing. Geophys. Res. Lett. 45, 1499−1508. https://doi.org/10.1002/2017GL076229.

Docquier, D., Massonnet, F., Barthélemy, A., et al., 2017. Relationships between Arctic sea ice drift and strength modelled by NEMO-LIM3.6. Cryosphere 11, 2829−2846. https://doi.org/10.5194/tc-11-2829-2017.

Döscher, R., Acosta, M., Alessandri, A., et al., 2022. The EC-Earth3 Earth system model for the coupled model Intercomparison Project 6. Geosci. Model Dev. (GMD) 15, 2973−3020. https://doi.org/10.5194/gmd-15-2973-2022.

Hakkinen, S., Proshutinsky, A., Ashik, I., 2008. Sea ice drift in the Arctic since the 1950s. Geophys. Res. Lett. 35, 19704. https://doi.org/10.1029/2008GL034791.

Kwok, R., Rothrock, D.A., 1999. Variability of Fram Strait ice flux and north Atlantic oscillation. J. Geophys. Res. Ocean. 104, 5177−5189. https://doi.org/10.1029/1998JC900103.

Kwok, R., Spreen, G., Pang, S., 2013. Arctic sea ice circulation and drift speed: decadal trends and ocean currents. J. Geophys. Res. Ocean. 118, 2408−2425. https://doi.org/10.1002/jgrc.20191.

Laxon, S.W., Giles, K.A., Ridout, A.L., et al., 2013. CryoSat-2 estimates of Arctic sea ice thickness and volume. Geophys. Res. Lett. 40, 732−737. https://doi.org/10.1002/grl.50193.

Lei, R., Heil, P., Wang, J., et al., 2016. Characterization of sea-ice kinematic in the Arctic outflow region using buoy data. Polar Res. 35, 22658. https://doi.org/10.3402/polar.v35.22658.

Li, X., Lu, R., Liu, J., et al., 2022. Comparison between large-scale circulation anomalies associated with interannual variability and decadal change of summer Arctic sea ice. J. Clim. 35, 4841−4858. https://doi.org/10.1175/JCLI-D-21-0803.1.

Olason, E., Notz, D., 2014. Drivers of variability in Arctic sea-ice drift speed. J. Geophys. Res. Ocean. 119, 5755−5775. https://doi.org/10.1002/2014JC009897.

Rampal, P., Weiss, J., Dubois, C., et al., 2011. IPCC climate models do not capture Arctic sea ice drift acceleration: consequences in terms of projected sea ice thinning and decline. J. Geophys. Res. Ocean. 116 (0−07). https://doi.org/10.1029/2011JC007110.

Rampal, P., Weiss, J., Marsan, D., 2009. Positive trend in the mean speed and deformation rate of Arctic sea ice, 1979−2007. J. Geophys. Res. 114, C05013. https://doi.org/10.1029/2008JC005066.

Rigor, I.G., Wallace, J.M., Colony, R.L., 2002. Response of sea ice to the Arctic oscillation. J. Clim. 15, 2648−2663. https://doi.org/10.1175/1520-0442(2002)015<2648:ROSITT>2.0.CO;2.

Schweiger, A., Lindsay, R., Zhang, J., et al., 2011. Uncertainty in modeled Arctic sea ice volume. J. Geophys. Res. Ocean. 116, C00D06. https://doi.org/10.1029/2011JC007084.

Sévellec, F., Fedorov, A.V., Liu, W., 2017. Arctic sea-ice decline weakens the Atlantic meridional overturning circulation. Nat. Clim. Change 7, 604−610. https://doi.org/10.1038/nclimate3353.

Smedsrud, L.H., Halvorsen, M.H., Stroeve, J.C., et al., 2017. Fram Strait sea ice export variability and September Arctic sea ice extent over the last 80 years. Cryosphere 11, 65−79. https://doi.org/10.5194/tc-11-65-2017.

Spreen, G., Kwok, R., Menemenlis, D., 2011. Trends in Arctic sea ice drift and role of wind forcing: 1992−2009. Geophys. Res. Lett. 38. https://doi.org/10.1029/2011GL048970.

Stroeve, J., Barrett, A., Serreze, M., et al., 2014. Using records from submarine, aircraft and satellites to evaluate climate model simulations of Arctic sea ice thickness. Cryosphere 8, 1839−1854. https://doi.org/10.5194/tc-8-1839-2014.

Tandon, N.F., Kushner, P.J., Docquier, D., et al., 2018. Reassessing sea ice drift and its relationship to long-term Arctic sea ice loss in coupled climate models. J. Geophys. Res. Ocean. 123, 4338−4359. https://doi.org/10.1029/2017JC013697.

Tremblay, L.B., Mysak, L.A., 1997. Modeling sea ice as a granular material, including the dilatancy effect. J. Phys. Oceanogr. 27, 2342−2360. https://doi.org/10.1175/1520-0485(1997)027<2342:MSIAAG>2.0.CO;2.

Vihma, T., 2014. Effects of Arctic sea ice decline on weather and climate: a review. Surv. Geophys. 35, 1175−1214. https://doi.org/10.1007/s10712-014-9284-0.

Watanabe, E., Wang, J., Sumi, A., et al., 2006. Arctic dipole anomaly and its contribution to sea ice export from the Arctic Ocean in the 20th century. Geophys. Res. Lett. 33. https://doi.org/10.1029/2006GL028112.

Wu, B., Wang, J., Walsh, J.E., 2006. Dipole anomaly in the winter Arctic atmosphere and its association with sea ice motion. J. Clim. 19, 210−225. https://doi.org/10.1175/JCLI3619.1.

Yu, X., Liu, C., Wang, X., et al., 2022. Evaluation of Arctic sea ice drift and its relationship with near-surface wind and ocean current in nine CMIP6 models from China. Adv. Atmos. Sci. 39, 903−926. https://doi.org/10.1007/s00376-021-1153-4.

Yu, X., Rinke, A., Dorn, W., et al., 2020. Evaluation of Arctic sea ice drift and its dependency on near-surface wind and sea ice conditions in the coupled regional climate model HIRHAM−NAOSIM. Cryosphere 14, 1727−1746. https://doi.org/10.5194/tc-14-1727-2020.

Zhang, F., Pang, X., Lei, R., et al., 2021. Arctic sea ice motion change and response to atmospheric forcing between 1979 and 2019. Int. J. Climatol. 42, 1854−1876. https://doi.org/10.1002/joc.7340.

Zhang, J., Rothrock, D.A., 2003. Modeling global sea ice with a thickness and enthalpy distribution model in generalized curvilinear coordinates. Mon. Weather Rev. 131, 845−861. https://doi.org/10.1175/1520-0493(2003)131<0845:MGSIWA>2.0.CO;2.